American Mineralogist, Volume 99, pages 2176–2186, 2014

MINERALS IN THE HUMAN BODY

Synthesis and structure of carbonated barium and lead fluorapatites: Effect of cation size on A-type carbonate substitution†

Zachary Wilt[1], Caitlyn Fuller[1], Taia Bachman[1], Victoria Weidner[1], Jill D. Pasteris[2] and Claude H. Yoder[1,*]

[1]Department of Chemistry, Franklin and Marshall College, Lancaster, Pennsylvania 17603, U.S.A.
[2]Department of Earth and Planetary Sciences, Washington University in St. Louis, St. Louis, Missouri 63130-4899, U.S.A.

Abstract

Substitution of carbonate has long been recognized in both synthetic and natural biologically and geologically precipitated forms of hydroxylapatite. Although the predominant substitution mechanism in all of the calcium members of the apatite group formed below 100 °C is substitution of carbonate for phosphate (B-type), small amounts of A-type substitution of carbonate in the channel sites also occur. The present study focuses on the effect of cation size on the type of substitution of carbonate in members of the apatite group. The barium and lead members offer a larger channel site, which potentially could stabilize A-type substitution. A series of carbonated barium and lead fluorapatites were synthesized in aqueous solution and characterized by powder X-ray diffraction, and infrared and Raman spectroscopy. Carbonate content was determined by combustion analysis.

Unit-cell parameters derived from X-ray diffraction showed that, as carbonate content increased, the **a**-axis length decreased and the **c**-axis increased slightly for carbonated barium fluorapatites (CBaApF), whereas the lengths of both the **a**- and **c**-axes increased for CPbApF. The co-occurrence of two sets of peaks in the ν_3 carbonate region of the infrared spectra of lead and barium carbonated apatites are strongly suggestive of both A- and B-type carbonate substitution. This interpretation is supported by Rietveld analysis of X-ray powder diffraction data, which confirms the presence of significant, but not dominant, A-type substituted carbonate ions. The variation in cell parameters as a function of carbonate substitution mode is discussed, and it is shown that B-type carbonate substitution need not be accompanied by a decrease in the **a**-axis in all apatites. The greater amount of A-type carbonate substitution in barium and lead fluorapatites compared to the their calcium homologs can be attributed to: (1) the less negative enthalpies of hydration of the barium and lead ions relative to that of calcium, and/or (2) the greater amount of space available for the relatively large carbonate ions in the channels defined by these large cations. Thus, the substitution modes can be controlled by either thermodynamic or kinetic considerations.

Keywords: Apatite, type A-carbonate, Rietveld, infrared, barium apatite, lead apatite

Introduction

Only five cations form well-characterized end-member apatites. These elements are the alkaline earth metals Ca, Sr, and Ba, the Group 14 metal Pb, and the transition metal Cd (Pan and Fleet 2002; Flora et al. 2004). The barium and lead apatites are particularly interesting because they contain the largest cations [the six-coordinate ionic radii for Ba^{2+} and Pb^{2+} are 1.35 and 1.19 Å, respectively, whereas the radius of Ca^{2+} is 1.00 Å (Shannon 1976)] present in end-member apatites and therefore can provide information on how cation size affects the structure and other characteristics of apatites. Of particular interest are the carbonated forms of these compounds because of the biological importance of the carbonated calcium homolog (CCaApOH), which is the mineral component of bones and teeth, and the possibility that larger cations may influence the substitution mode of carbonate. The barium and lead apatites are also of interest because of their formation in the remediation of heavy metal spills using phosphate remediants (Nriagu 1984; Ruby et al. 1994; Traina and Laperche 1999). We have previously reported on the preparation and characterization of lead hydroxyl- and chlorapatites (pyromorphites) (Sternlieb et al. 2010) as well as barium hydroxyl- and chlorapatites (Yoder et al. 2012).

Carbonate can be incorporated in the apatite structure in two different ways. In A-type substitution, carbonate resides in the channels between the M(2) metal ions, as represented, for example, by the formula $Ca_{10}(PO_4)_6(CO_3)_x(F)_{2-2x}$. In B-type substitution, carbonate replaces a phosphate ion. Both types of substitution require charge compensation due to the difference in charge between the carbonate ion and the ions it replaces. In A-type substitution the charge is generally compensated by the removal of two fluoride ions for each substituting carbonate. There

* E-mail: claude.yoder@fandm.edu
† Special collection papers can be found on GSW at http://ammin.geoscienceworld.org/site/misc/specialissuelist.xhtml.

0003-004X/14/1112–2176$05.00/DOI: http://dx.doi.org/10.2138/am-2014-4827

is evidence for two positions of carbonate in the channels—the plane of A1 carbonate ions is parallel to the **c**-axis, while the plane of A2 carbonate ions is nearly perpendicular to the **c**-axis. A2 substitution appears to be correlated with substitution of carbonate for phosphate (Fleet and Liu 2004; Tacker 2008). For B-type substitution various charge-compensation mechanisms have been proposed (Pan and Fleet 2002), but the two most likely for apatites prepared in aqueous solution are (1) paired creation of divalent cation and monovalent anion vacancies and (2) substitution of sodium ions for channel calcium ions in solutions bearing sodium reagents (Pan and Fleet 2002). The more common mechanism of charge-compensation with vacancy of both a channel metal ion and a monovalent channel anion for B-type substitution is represented, for example, as $Ca_{10-x}(PO_4)_{6-x}(CO_3)_x(F)_{2-x}$. For calcium hydroxyl- and fluorapatites precipitated at temperatures from 20 to 100 °C in aqueous solution, B-type substitution predominates, although some A-type substitution, typically <15% of all carbonate (Elliott 2002), is generally also present. B-type substitution produces a decrease in the *a* unit-cell dimension with increasing carbonate incorporation. This change in the **a**-axis length as a function of carbonate content, as observed in calcium fluor- and hydroxylapatites, has become an important criterion for recognizing the substitution type—a decrease in **a**-axis length for B-type substitution and an increase in **a**-axis length for A-type substitution. (LeGeros et al. 1969; Elliott 1994; Pan and Fleet 2002)

Although at least one study has been performed on samples of barium fluorapatite synthesized at high temperature (Meegoda et al. 1999), there appears to be only one report of a synthesis for this apatite in aqueous solution (Flora et al. 2004). Syntheses of lead fluorapatite in aqueous solution (Bhatnagar 1970) and in the solid state (Liu et al. 2008) have been reported.

Our objectives in this study were to prepare barium and lead fluorapatites with varying degrees of carbonation and to determine the substitution mode employed by these compounds to incorporate carbonate. Of particular interest to us was the effect of the nature and size of the cation on the distribution of carbonate in the apatite structure. We have used infrared and Raman spectroscopy as well as Rietveld analysis of XRD patterns to characterize the samples and to determine the location of the carbonate ion in the apatite structure.

EXPERIMENTAL METHODS

All syntheses utilized Milli-Q deionized water through which N_2 had been bubbled for at least 6 h to remove CO_2. Reagents were ACS reagent grade of purity higher than 98%.

Synthesis of carbonated BaApF

To minimize exposure to atmospheric CO_2, syntheses were performed under a positive pressure of argon, and suction filtration and drying were done in a nitrogen-filled glove bag. Solutions of NH_4F and $(NH_4)_2HPO_4$ were combined before addition of other components. A solution of the metal nitrate and the solution of NH_4F and $(NH_4)_2HPO_4$ were added simultaneously to a solution of $NaHCO_3$ maintained at 80–90 °C. The amount of $NaHCO_3$ was varied to produce apatites with different concentrations of carbonate. Before titration, the pH of the carbonate bath was adjusted to pH 12 using 6 M NaOH solution. During the titration at a rate of 0.05 mL/s, the solution was stirred and the pH was maintained at 12. After ca. 3 h, the reaction mixture was allowed to sit for 16 h at 85 °C with stirring, under nitrogen. After cooling, the white precipitate was suction filtered in a glove bag using a medium porosity filter crucible, washed thoroughly with three portions of water, allowed to aspirate for an hour, dried with nitrogen in a glove bag for 16 h, and finally heated in a 140 °C oven for 1 h. Percent yields were generally above 80%.

For the preparation of an apatite using a mole ratio of carbonate to phosphate of 0.5 to 1 the following masses of reagents and volumes of water were used for solution preparation: $NaHCO_3$, 0.1345 g, 20 mL; NH_4F, 0.0793 g, 10 mL; $(NH_4)_2HPO_4$, 0.4248 g, 10 mL; $Ba(NO_3)_2$, 1.4018 g, 20 mL.

Synthesis of CPbApF

Portions (25 mL) of solutions of 0.15 M $Pb(NO_3)_2$, 0.06 M NH_4F, and 0.09 M $NH_4H_2PO_4$ were titrated into 100 mL of water at a rate of about 0.7 mL/min. To the solution, 25 mL of different NH_4HCO_3 concentrations were titrated at a rate of 0.7 mL/min to obtain different carbonate/phosphate ratios. The NH_4HCO_3 solution was added at the same time as the other reagents. As the reagents were added, the solution was heated to 80 °C, brought to pH 9, and stirred magnetically. The pH was held at 9 throughout the synthesis with 6 M NH_3. After all of the reagents were added, the solution was digested for 2 h and then was suction filtered. The reaction mixture was filtered using a fine porosity glass filter crucible and was washed with three portions of water. The sample was then dried in vacuo in a vacuum desiccator for over 24 h. Yields were 80–95%.

Compositional and structural analyses of samples

Powder X-ray diffractograms were obtained using a PANalytical X'Pert PRO multi-purpose diffractometer (MPD) Theta-Theta System with Cu$K\alpha$ radiation. A step size of 0.02° 2θ was used with a range from 5 to 90° 2θ. X-ray diffraction was used to confirm the identity of the compound, to detect other phases present in the samples, and to provide data for Rietveld analyses. Data for Rietveld analyses were collected with the sample in a 10 mm silicon cavity mount and scans (ca. 5–8 h) sufficient to obtain 60 000 to 100 000 counts.

Unit-cell parameters were determined both during Rietveld analyses and by using profile-fitting of the entire XRD pattern. The indexing method was usually McMaille (Le Bail 2004), but in some cases the Treor method (Werner et al. 1985) was employed. The unit-cell candidate was chosen based on its high figure of merit, symmetry, and absence of unindexed peaks. Uncertainties in unit-cell parameters were generally ±0.0007, but repeated measurements on the same sample suggest a higher uncertainty of ca. ±0.001 Å.

Weight percent carbon, lead, phosphorus, and fluoride were all determined by Galbraith Laboratories, Knoxville, Tennessee. Weight percent carbon was determined using a C-, H-, N- elemental analyzer after combustion at 950 °C in oxygen. The reported carbon concentrations have a relative experimental error of ±0.3 wt%. Infrared spectra were obtained using a Ge ATR sample mount on a Bruker Tensor 37 IR spectrometer. Each spectrum represents 256 scans at a resolution of 2 cm^{-1}.

The confocal Raman system from Kaiser Optical (Ann Arbor, Michigan) that was used in this study has an integrated, fiberoptically coupled microscope-spectrometer-detector. The HoloLab Series Research Raman spectrometer is configured for 532 nm laser excitation and simultaneously records the spectral range of 100 to 4000 Δcm^{-1}. The detector is an Andor high-resolution, thermoelectrically cooled CCD array that provided a resolution of 2.5 cm^{-1}. Powders were analyzed using an Olympus 80× objective with an N.A. of 0.75. Each Raman spectrum is the average of 32 acquisitions of 4 s each. Every sample underwent at least 6 analyses. The laser power was 10 mW at the sample surface, and the diameter of the beam was about 1 μm at the sample surface. The focus was adjusted for maximum signal:noise ratio.

The presence of fluoride was ascertained using ^{19}F NMR spectroscopy to determine the relative amount of fluoride in several apatites, previously dissolved in nitric acid. A sample of NaF in the same concentration of acid was used as a standard. Spectra were obtained on an Agilent INOVA 500 MHz spectrometer at 25 °C.

Rietveld analysis

The Panalytical program X'pert Highscore Plus (version 2.2e) was used to perform Rietveld analyses on all samples. The profile function was pseudo-Voigt with a polynomial background including 5 coefficient parameters and a flat background parameter. The initial models for $P6_3/m$ calcium fluorapatite (Sudarsanan et al. 1972), barium fluorapatite (Mayer et al. 1979), and lead fluorapatite (Belokoneva et al. 1982) were obtained from published single-crystal X-ray diffraction data. In all refinements, the zero-shift, scale factor, all 5 background coefficients, unit-cell parameters, and profile parameters were refined. It was assumed that both B- and A-type substitution could occur within the same unit cell. The possibility of both types of substitution, either independently or as a mixture of both is well documented (Beshah et al. 1990; Schramm et al. 2001; Tonegawa et al. 2010; Ikoma et al. 2000; Fleet et al. 2004; Astala and Stott 2005; Fleet and Liu 2005; Resende et al. 2006; Nassif et al. 2010). For B-type carbonate the model developed by Wilson et al. (2004) was adopted: the planar carbonate ion was assumed to occupy a face

of the tetrahedron that otherwise would have been a phosphate ion, with two of carbonate's oxygen atoms in similar positions to those of the phosphate's oxygen atoms. The occupancies of these two O atoms were not refined. A-type carbonate was assumed to be centered at the position 0, 0, 0.5 with two of the oxygen atoms of the trigonal planar carbonate ion located close to the z-axis, as discussed by Fleet and Liu (2005) as the A1 type carbonate. The occupancies of the carbon and its corresponding oxygen sites in A-type substitution were constrained so that the magnitudes of their values changed together.

To develop a starting model for the refinements, the occupancies were set to values obtained from the formula for B-type substitution as calculated from the analytically determined carbonate percentage. These occupancies were then refined, which allowed for a refinement independent of the data obtained from chemical analysis. The occupancies of the carbon and phosphorus could be determined with a lack of divergence, but these occupancies exhibited a great deal of uncertainty. The position of the monovalent anion along the z-axis and its site occupancy were refined in all apatites. The bond lengths in the phosphate tetrahedra and other atomic distances obtained by refinement were very close to those in the starting model. Throughout all refinements, the agreement indices were monitored to be sure that the system was not diverging and that the refinement was moving toward a reasonable representation of the actual structure.

Results and discussion

Syntheses

The preparation of both the lead and barium carbonated fluorapatites was accomplished by addition of phosphate and fluoride to a solution of the cation at a pH of 9 and 12, respectively. It is believed that these pH values are optimal. The low solubility of the carbonated lead apatites allows for the formation of those compounds under conditions where the concentration of PO_4^{3-} ion is low. The greater solubility of the barium compared to the lead apatites requires higher pH values to ensure higher concentrations of phosphate. Of course, the much greater solubility of $Ba(OH)_2$ relative to $Pb(OH)_2$ also permits the use of higher pH values in the synthesis of the barium apatites.

X-ray diffraction

The powder X-ray diffraction patterns of carbonated barium fluorapatites show little change in either position or breadth of the peaks with increasing carbonate content. The full-width at half maximum (FWHM) for two barium fluorapatites containing 1.3 and 3.0 wt% carbonate were 0.10 and 0.17° 2θ, respectively, for the 300 line and 0.20 and 0.20° 2θ, respectively, for the 113 line. In contrast, the lead fluorapatites show a relatively small change in the breadth of the peaks, but a definite shift in multiple peak positions to higher 2θ values as the carbonate content increases. For lead fluorapatites containing 1.5 and 3.0 wt% carbonate the FWHM values for the 112 peak were 0.25 and 0.30° 2θ, respectively, and for the 300 peak 0.32 and 0.37° 2θ, respectively. Therefore, unlike their calcium analogs, which show significant peak broadening with increased carbonate content (Nelson and Williamson 1982; Rey et al. 1991), the barium and lead analogs apparently do not undergo major changes in crystallite size and internal strain as carbonate percentages increase. This lack of significant peak broadening was also observed for carbonated barium hydroxyl- and chlorapatites (Yoder et al. 2012).

Unit-cell parameters

The unit-cell parameters obtained for CBaApF are shown in Figure 1, which demonstrates a decrease in the **a**-axis length of about 0.05 Å and a more scattered, but probable increase in **c**-axis length of about 0.01 Å over a range of ca. 3 wt% carbonate.

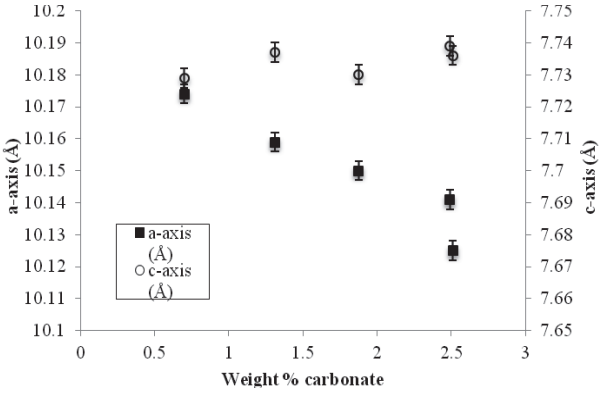

Figure 1. Variation of unit-cell parameters as a function of weight percent carbonate in CBaApF.

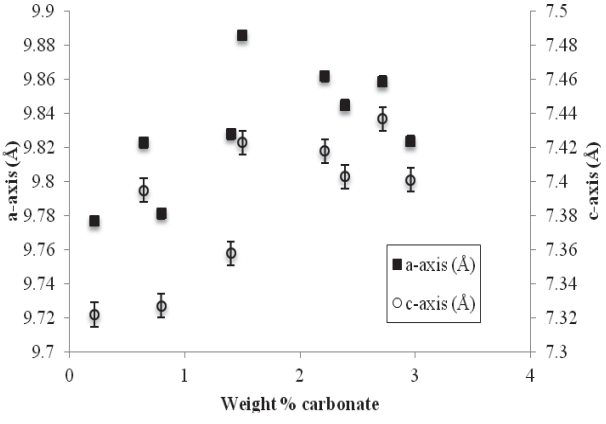

Figure 2. Variation of unit-cell parameters as a function of weight percent carbonate in CPbApF.

For CPbApF, the unit-cell parameters (Fig. 2) show an increase in both axes and hence an increasing cell volume as carbonate content increases, consistent with the observed shifts in all XRD peaks to lower 2θ values.

A decrease in **a**-axis length was observed previously for CBaApCl, CBaApOH, and CPbApCl, but not in CPbApOH (Yoder et al. 2012; Sternlieb et al. 2010). The decrease in **a**-axis length for CBaApF could be attributed to B-type substitution of carbonate for phosphate, as observed for calcium apatites, but Rietveld analysis and IR spectroscopy (see below) indicate the likelihood of significant A-type substitution (Holcomb and Young 1980; Elliott 2002; Tonegawa et al. 2010; Fleet et al. 2004).

Raman spectra

The Raman spectra of the same samples also show clearly defined peaks for P-O and C-O vibrations. Figure 3 displays the 870 to 1100 Δcm^{-1} region for five CPbApF samples of different carbonate composition. The peaks at 927–933 Δcm^{-1} correspond to the ν_1 symmetric P-O stretching mode and those at 948–967 Δcm^{-1} to the ν_3 asymmetric P-O stretching mode. The intensity of the peaks in the 1039–1050 Δcm^{-1} range correlate with the concentration of carbonate in the samples. All the above peaks

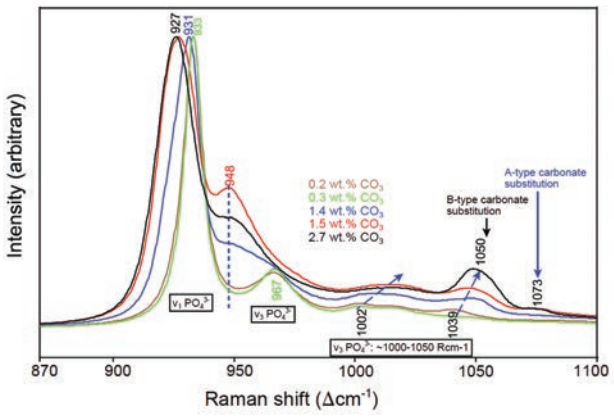

FIGURE 3. Raman spectra for five CPbApF samples of varying carbonate composition. (Color online.)

are approximately 30 cm^{-1} lower than the corresponding peaks in the calcium analogs, indicating that the cation mass difference controls the relative peak positions. Reference to carbonated hydroxylapatite, CCaApOH (Penel et al. 1998), indicates that the peak at ~1050 Δcm^{-1} can be assigned to B-type carbonate substitution, which is the dominant substitution mechanism recorded in all the Raman spectra. The CPbApF spectra in Figure 3 show not only an increase in intensity of the ~1050 Δcm^{-1} peak with increasing carbonation but also a gradual upshift in peak position, from ~1039 Δcm^{-1} in the uncarbonated apatite. Similar spectral behavior occurs in CCaApOH samples of increasing carbonate concentration, although in that case the carbonate peak downshifts several wavenumbers (Wopenka and Pasteris 2005). These two peak-shift responses are unexpected for a simple ν_1 C-O symmetric stretch, as each of the carbonate-correlated peaks is often assigned. Instead, the change in peak position in response to additional carbonate incorporation is more suggestive of a band that reflects the interaction between two modes, i.e., a ν_1 C-O and a ν_3 P-O mode (Nelson and Williamson 1982; Penel et al. 1998; Wopenka and Pasteris 2005; Awonusi et al. 2007). In analogy with CCaApOH (Nelson and Williamson 1982; Penel et al. 1998), the weak peak at 1073 Δcm^{-1} is assigned to A-type carbonate, and several other peaks at lower frequency may represent A-type substitution. The Raman spectral response of PbApF to increasing degrees of carbonation is similar to that of CPbApOH (Sternlieb et al. 2010) except for the much greater shift of the ν_1 and ν_3 P-O peak positions in CPbApF. Both CPbApOH and CPbApF show peaks for both A- and B-type carbonate substitution, with B-type strongly dominant.

All of the CPbApF samples also show a broad water peak at about 3400 Δcm^{-1} that dominantly records adsorbed water, but also shows some structural water (Pasteris et al. 2014). A weak sharp peak at 3570 Δcm^{-1} (not shown) in the least carbonated samples corresponds to OH^- ions that presumably occupy the channel. For comparison, the O-H stretch in hydrocerrusite is at 3537 Δcm^{-1}, whereas the O-H stretch in hydroxylapatite is at 3572 Δcm^{-1} and in PbApOH at 3561 Δcm^{-1} (Sternlieb et al. 2010). The presence of fluoride in the channel site of an OH-bearing apatite phase will displace the O-H stretch peak. Fluoride typically downshifts the peak position due to strong hydrogen bonding in the OH-F interaction, whereas carbonate substitution causes upshift in the O-H stretch of CCaApOH (Pasteris et al. 2012). Thus, the position of the OH peak shown by the least-carbonated CPbApF samples may reflect two opposing deflections.

In the Raman spectra of CBaApF (Fig. 4), the ν_1 P-O stretching mode appears at about the same location as that in CPbApF (935 Δcm^{-1} for CBaApF), but the former's peak position is relatively insensitive to the concentration of carbonate in the sample. However, the width of the ν_1 P-O stretching mode increases as carbonate content increases. This spectral response is similar to that of CBaApOH (Yoder et al. 2012). In CBaApF, the ν_3 mode at 1030 Δcm^{-1} is better resolved than in CPbApF. The intensity of the 1058 Δcm^{-1} peak again indicates the dominance of B-type carbonate substitution compared to the shoulder at ~1075 Δcm^{-1}, which appears to represent A-type substitution.

The inset in Figure 4 makes clearer the sensitive intensity response of the 1058 Δcm^{-1} peak to carbonate substitution, as well as the slight peak shifts among the ν_3 modes at lower wavenumbers. As with the lead apatites, CBaApF exhibits a broad peak (not shown) centered at about 3400 Δcm^{-1} for the OH stretching of water (mostly adsorbed), but its intensity is not significant except in the most highly carbonated sample. There is no evidence of OH^- ions.

The Raman spectra of the two sets of samples confirm the purity of the CPbApF and CBaApF powders. Both phases show a significant component of A-type carbonate substitution (not readily quantifiable), but B-type substitution strongly dominates in both. The CPbApF phase shows a greater degree of structural/atomic disorder in response to carbonate substitution than does the CBaApF, as indicated by the greater peak-broadening in the former. The large amount (6 cm^{-1}) of shift in the position of the ν_1 P-O peak in CPbApF (Fig. 3) also indicates significant change in the phosphate environment due to carbonate substitution, further distinguishing it from CBaApF. In this regard, the Raman data are consistent with the comparative XRD results on the two phases.

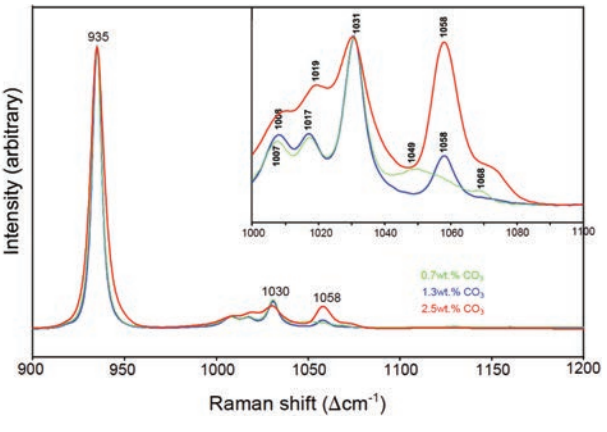

FIGURE 4. The 900–1200 Δcm^{-1} region of the Raman spectra of three CBaApF samples. In the inset, the peaks are normalized to the intensity of the ν_3 mode at 1031 Δcm^{-1}, making more clear the increase in intensity of the 1058 Δcm^{-1} peak representing B-type substitution. (Color online.)

TABLE 1. Rietveld refinement parameters and site occupancies for cations and monovalent anions

Compound	wt% CO_3	Ion CO_3/ unit cell	Total counts: difference ratio	R_{wp} (%)	M_1 occupancy	M_1 B_{iso}	M_2 occupancy	M_2 B_{iso}	X ions/ unit cell
CCaApF	1.45	0.24	5	7.53	1.13(7)	2.5(1)	0.88(6)	0.0(1)	1.6(2)
CCaApF	4.23	0.67	6	6.23	1.13(7)	2.5(2)	0.91(8)	0.0(1)	1.8(2)
CCaApF	13.55	1.88	12.5	4.58	1.11(7)	3.1(1)	0.96(8)	0.9(1)	1.2(2)
CBaApF	0.70	0.23	25	5.04	0.94(9)	0.28(5)	0.92(9)	0.14(4)	1.2(4)
CBaApF	1.31	0.42	13	6.17	1.0(1)	0.68(5)	1.0(1)	0.63(4)	1.2(4)
CBaApF	2.51	0.77	16	6.15	0.9(1)	0.38(5)	0.9(1)	0.57(5)	0.6(4)
CPbApF	0.22	0.10	23	4.51	1.0(2)	0.41(5)	1.0(2)	0.94(4)	1.6(8)
CPbApF	1.59	0.67	21	7.20	1.0(2)	0.97(9)	0.9(2)	1.22(8)	1.0(8)
CPbApF	2.72	1.09	70	4.04	1.0(1)	0.69(4)	0.9(1)	1.35(4)	1.0(4)

TABLE 2. Selected bond lengths obtained in the Rietveld refinements

Compound	wt% CO_3	P_1–O_1 (Å)	P_1–O_2 (Å)	P_1–O_3 (Å)	M_1–O_1 (Å)	M_1–O_2 (Å)	M_1–O_3 (Å)	M_2–X (Å)	M_2–O_2 (Å)	M_2–O_3 (Å)
CCaApF	1.45	1.5385(2)	1.5454(2)	1.5364(2)	2.403(3)	2.454(3)	2.809(1)	2.332(3)	2.366(3)	2.338(1)
CCaApF	4.23	1.5321(2)	1.5390(2)	1.5347(2)	2.396(4)	2.453(4)	2.798(1)	2.293(3)	2.384(3)	2.344(1)
CCaApF	13.55	1.5233(2)	1.5302(2)	1.5331(2)	2.372(4)	2.467(4)	2.787(1)	2.293(3)	2.363(3)	2.340(1)
CBaApF	0.70	1.5382(2)	1.5330(2)	1.5329(2)	2.725(2)	2.710(2)	>3	2.525(1)	2.663(1)	2.739(1)
CBaApF	1.31	1.5370(2)	1.5318(2)	1.5332(2)	2.726(3)	2.710(3)	>3	2.524(1)	2.659(1)	2.741(1)
CBaApF	2.51	1.5336(2)	1.5284(2)	1.5327(2)	2.726(3)	2.706(3)	>3	2.494(1)	2.675(1)	2.747(1)
CPbApF	0.22	1.5564(2)	1.5435(2)	1.5869(2)	2.510(1)	2.728(1)	2.911(1)	2.939(1)	2.383(1)	2.562(1)
CPbApF	1.59	1.5641(2)	1.5511(2)	1.6028(2)	2.52(1)	2.76(1)	2.929(4)	>3	2.322(4)	2.595(2)
CPbApF	2.72	1.5700(2)	1.5570(2)	1.6094(2)	2.542(6)	2.764(5)	2.937(1)	>3	2.309(2)	2.600(1)

TABLE 3. Site occupancies and atomic coordinates for atoms in synthesized CMApF

							Coordinates		
Compound	ID	wt% CO_3^{2-}	Ions CO_3^{2-} per cell	Site	Wyckoff symbol	Occup.	x	y	z
CCaApF	DSCaApF13	1.45	0.24						
				C1	12*i*	0.01(2)	0.014000	0.010000	0.019000
				C2	12*i*	0.0(1)	0.419700	0.013700	0.187000
				Ca1	4*f*	1.13(7)	0.333333	0.666667	0.0006(7)
				Ca2	6*h*	0.88(6)	0.2429(4)	0.2532(4)	0.250000
				F1	2*a*	0.8(1)	0.000000	0.000000	0.250000
				O1	6*h*	1.000000	0.158100	0.484300	0.250000
				O2	6*h*	1.000000	0.588000	0.121200	0.250000
				O3	12*i*	0.8(1)	0.341600	0.084800	0.070400
				O5	12*i*	0.01(2)	0.105000	0.166500	0.002000
				O6	12*i*	0.01(2)	0.021000	0.051000	0.187000
				O7	12*i*	0.01(2)	0.073000	0.001000	0.128200
				P1	6*h*	0.916064	0.398100	0.029300	0.250000
CCaApF	DSCaApF1	4.23	0.67						
				C1	12*i*	0.00(2)	0.014000	0.010000	0.019000
				C2	12*i*	0.0(1)	0.419700	0.013700	0.187000
				Ca1	4*f*	1.13(7)	0.333333	0.666667	0.0013(8)
				Ca2	6*h*	0.91(8)	0.2395(4)	0.2502(5)	0.250000
				F1	2*a*	0.9(1)	0.000000	0.000000	0.250000
				O1	6*h*	1.000000	0.158100	0.484300	0.250000
				O2	6*h*	1.000000	0.588000	0.121200	0.250000
				O3	12*i*	0.79(8)	0.341600	0.084800	0.070400
				O5	12*i*	0.00(2)	0.105000	0.166500	0.002000
				O6	12*i*	0.00(2)	0.021000	0.051000	0.187000
				O7	12*i*	0.00(2)	0.073000	0.001000	0.128200
				P1	6*h*	0.8(1)	0.398100	0.029300	0.250000
CCaApF	DSCaApF9	13.55	1.88						
				C1	12*i*	0.02(2)	0.014000	0.010000	0.019000
				C2	12*i*	0.148461	0.419700	0.013700	0.187000
				Ca1	4*f*	1.11(7)	0.333333	0.666667	0.0051(8)
				Ca2	6*h*	0.96(8)	0.2403(4)	0.2523(5)	0.250000
				F1	2*a*	0.6(1)	0.000000	0.000000	0.250000
				O1	6*h*	1.000000	0.158100	0.484300	0.250000
				O2	6*h*	1.000000	0.588000	0.121200	0.250000
				O3	12*i*	0.7(1)	0.341600	0.084800	0.070400
				O5	12*i*	0.02(2)	0.105000	0.166500	0.002000
				O6	12*i*	0.02(2)	0.021000	0.051000	0.187000
				O7	12*i*	0.02(2)	0.073000	0.001000	0.128200
				P1	6*h*	0.71(6)	0.398100	0.029300	0.250000
CBaApF	CT5	0.70	0.23						
				Ba1	4*f*	0.94(9)	0.333333	0.666667	0.0006(4)
				Ba2	6*h*	0.92(9)	0.2571(1)	0.2391(1)	0.250000
				C1	12*i*	0.04(2)	0.018000	0.065000	0.008000
				C2	12*i*	0.1(2)	0.017800	0.419600	0.198000
				F1	2*a*	0.6(2)	0.000000	0.000000	0.250000
				O1	6*h*	1.000000	0.482000	0.140400	0.250000
				O2	6*h*	1.000000	0.117400	0.576000	0.250000

(Continued on next page)

TABLE 3.—*CONTINUED*

Compound	ID	wt% CO_3^{2-}	Ions CO_3^{2-} per cell	Site	Wyckoff symbol	Occup.	Coordinates x	Coordinates y	Coordinates z
CBaApF	CT5	0.70	0.23						
				O3	12*i*	1.0(1)	0.079100	0.347300	0.088800
				O5	12*i*	0.04(2)	0.084000	0.208900	0.028000
				O6	12*i*	0.04(2)	0.007000	0.023000	0.143000
				O7	12*i*	0.04(2)	0.022000	0.008000	0.139000
				P1	6*h*	1.0(2)	0.031900	0.401700	0.250000
CBaApF	CT2	1.31	0.42						
				Ba1	4*f*	1.0(1)	0.333333	0.666667	0.0007(5)
				Ba2	6*h*	1.0(1)	0.2571(1)	0.2394(1)	0.250000
				C1	12*i*	0.04(2)	0.018000	0.065000	0.008000
				C2	12*i*	0.2(2)	0.017800	0.419600	0.198000
				F1	2*a*	0.6(2)	0.000000	0.000000	0.250000
				O1	6*h*	1.000000	0.482000	0.140400	0.250000
				O2	6*h*	1.000000	0.117400	0.576000	0.250000
				O3	12*i*	1.0(1)	0.079100	0.347300	0.088800
				O5	12*i*	0.04(2)	0.084000	0.208900	0.028000
				O6	12*i*	0.04(2)	0.007000	0.023000	0.143000
				O7	12*i*	0.04(2)	0.022000	0.008000	0.139000
				P1	6*h*	0.9(2)	0.031900	0.401700	0.250000
CBaApF	CT7	2.51	0.77						
				Ba1	4*f*	0.9(1)	0.333333	0.666667	0.0011(5)
				Ba2	6*h*	0.9(1)	0.2548(2)	0.2370(2)	0.250000
				C1	12*i*	0.07(3)	0.018000	0.065000	0.008000
				C2	12*i*	0.3(2)	0.017800	0.419600	0.198000
				F1	2*a*	0.3(2)	0.000000	0.000000	0.250000
				O1	6*h*	1.000000	0.482000	0.140400	0.250000
				O2	6*h*	1.000000	0.117400	0.576000	0.250000
				O3	12*i*	1.0(1)	0.079100	0.347300	0.088800
				O5	12*i*	0.07(3)	0.084000	0.208900	0.028000
				O6	12*i*	0.07(3)	0.007000	0.023000	0.143000
				O7	12*i*	0.07(3)	0.022000	0.008000	0.139000
				P1	6*h*	0.8(2)	0.031900	0.401700	0.250000
CPbApF	ZW11	0.22	0.10						
				C1	12*i*	0.06(3)	0.018000	0.065000	0.008000
				C2	12*i*	0.3(3)	0.412000	0.004000	0.187000
				F1	2*a*	0.000000	0.000000	0.000000	0.250000
				O1	6*h*	1.000000	0.164000	0.487000	0.250000
				O2	6*h*	1.000000	0.582000	0.096000	0.250000
				O3	12*i*	0.8(2)	0.347000	0.080000	0.078000
				O5	12*i*	0.06(3)	0.068200	0.212200	0.028000
				O6	12*i*	0.06(3)	0.007000	0.005000	0.152000
				O7	12*i*	0.06(3)	0.024000	0.010000	0.148000
				P1	6*h*	0.9(2)	0.400400	0.019100	0.250000
				Pb1	4*f*	0.8(1)	0.333333	0.666667	–0.001(2)
				Pb2	6*h*	0.8(1)	0.2376(3)	0.2348(3)	0.250000
CPbApF	ZW12	1.59	0.67						
				C1	12*i*	0.06(4)	0.018000	0.065000	0.008000
				C2	12*i*	0.3(4)	0.412000	0.004000	0.187000
				F1	2*a*	0.000000	0.000000	0.000000	0.250000
				O1	6*h*	1.000000	0.164000	0.487000	0.250000
				O2	6*h*	1.000000	0.582000	0.096000	0.250000
				O3	12*i*	0.7(2)	0.347000	0.080000	0.078000
				O5	12*i*	0.06(4)	0.068200	0.212200	0.028000
				O6	12*i*	0.06(4)	0.007000	0.005000	0.152000
				O7	12*i*	0.06(4)	0.024000	0.010000	0.148000
				P1	6*h*	0.8(3)	0.400400	0.019100	0.250000
				Pb1	4*f*	0.8(2)	0.333333	0.666667	–0.001(2)
				Pb2	6*h*	0.8(2)	0.2491(6)	0.2485(5)	0.250000
CPbApF	ZW3	2.72	1.09						
				C1	12*i*	0.06(3)	0.018000	0.065000	0.008000
				C2	12*i*	0.1(3)	0.412000	0.004000	0.187000
				F1	2*a*	0.000000	0.000000	0.000000	0.250000
				O1	6*h*	1.000000	0.164000	0.487000	0.250000
				O2	6*h*	1.000000	0.582000	0.096000	0.250000
				O3	12*i*	0.7(1)	0.347000	0.080000	0.078000
				O5	12*i*	0.06(3)	0.068200	0.212200	0.028000
				O6	12*i*	0.06(3)	0.007000	0.005000	0.152000
				O7	12*i*	0.06(3)	0.024000	0.010000	0.148000
				P1	6*h*	1.0(2)	0.400400	0.019100	0.250000
				Pb1	4*f*	1.0(1)	0.333333	0.666667	–0.003(1)
				Pb2	6*h*	0.9(1)	0.2472(4)	0.2474(3)	0.250000

Rietveld analysis

Tables 1–3 show the results of Rietveld analyses of the XRD patterns of three series of apatites (CCaApF, CBaApF, and CPbApF) containing low, medium, and high percentages of carbonate. Our Rietveld analyses for three CCaApF apatites were included to provide a control group to demonstrate the general validity of the models used. The atomic coordinates obtained in these analyses are provided in Table 3, and a summary of refinement parameters, cation occupanicies, and bond lengths based on the Rietveld results are given in Tables 1 and 2. In Table 1 the column "Total counts/difference counts" provides a ratio of the maximum counts of the experimental XRD pattern to the maximum counts obtained when the pattern developed by the refinement is subtracted from the experimental pattern. This is a measure of the agreement between the experimental and refinement-based X-ray patterns. A more widely used agreement index is R_{wp}, for which values below 6 or 7% are generally considered to be indicative of satisfactory fits of the data (Wilson et al. 2006, 2004, 2005): the lower the R_{wp} value, the better the fit produced by the refinement. The most important columns in these tables are those that give the occupancies of all of the sites in the refined structure. For the ideal end-member BaApF [$Ba_{10}(PO_4)_6F_2$], the occupancies of each of the two types of barium sites—Ba(1) and Ba(2)—should be exactly 1.000, meaning that all four possible Ba(1) ions and all six Ba(2) ions are present in the unit cell. The total number of each type of atom can be obtained by multiplying the occupancy by the numerical part of the Wykoff symbol for the atom site (see Table 3).

For the carbonated apatites prepared in this study, it is important to remember that each B-type substitution replaces one phosphate ion with one carbonate ion and (according to the accepted mechanism) results in the loss or vacancy of one calcium ion and one monovalent ion to maintain charge neutrality. A-type substitution, on the other hand, results in the displacement of two monovalent channel anions for each substituting carbonate ion. Hence, pure A-type substitution does not change the occupancies of the cation sites, which would remain at 1.000, but decreases the occupancies of the monovalent (X) ions. The type of substitution is also monitored by the occupancies of the two types of carbons belonging to the two structurally distinct types of carbonate ion that could be present in the structure—C1 (A1-type carbonate in the anion channel) and C2 (B-type carbonate in the phosphate site).

Thus, for the most-carbonated calcium control sample CCaApF Table 3 shows occupancies of 0.02(2) for C1 (total of 0.24 A-type carbonate ions), 0.15 for C2 (total of 1.9 B-type carbonate ions), 1.11(7) for Ca1 (total of 4.44 Ca1 cations), 0.96(8) for Ca2 (total of 5.76 Ca2 cations), 0.6(1) for F1 (total of 1.2 fluoride ions), and 0.71(6) for P1 (total of 4.4 phosphate ions). The occupancies for C1 and C2 indicate predominant B-type substitution as does the presence of 4.4 phosphate ions, but the high occupancies of the two types of calcium sites indicate A-type substitution, in which no cations are lost. Table 1 also indicates, however, that the isotropic thermal B_{iso} values for these cations, particularly Ca1, are very high. High B_{iso} values are generally an indication of high uncertainty in the position and occupancy of an atom. We therefore give less credence to the Ca1 site occupancy and note that substitution of 1.9 B-type carbonate ions (as indicated by the C2 occupancy) should result in loss of the same number of phosphate ions. Hence, the P1 occupancy should be about 6 – 1.9 = 4.1, in acceptable agreement with the value of 4.4 phosphate ions. The large uncertainties associated with each occupancy are also indicative of a great deal of uncertainty in the position of the carbonate in the final refined structure.

Because the most carbonated samples of CBaApF and CPbApF most clearly show A-type substitution in their infrared spectra (see below), we will only analyze the Rietveld occupancies of these two apatites. Thus, CBaApF containing 2.51 wt% carbonate shows significant occupancy of the channel C1 site [0.07(3)], though this occupancy is only one-quarter that of the B-type C2 site [0.3(2)]. There are also large uncertainties associated with both values. The two barium ion site occupancies of 0.9 each indicate a total vacancy of one barium ion, probably produced by B-type substitution. The fluoride occupancy of 0.3 represents 1.4 fluorine site vacancies, which is consistent with both A- and B-type substitution. The phosphorus occupancy of 0.8 corresponds to 1.2 phosphate vacancies, corresponding to dominant B-type substitution.

For CPbApF containing 2.72 wt% carbonate, the refinement produced one of the largest C1/C2 site occupancy ratios (0.06/0.1), and thus the largest A- to B-type substitution ratios. Even in this case, however, A-type substitution is only about half that of B-type substitution. The "high" P1, Pb1, and Pb2 and low F1 occupancies are consistent with a significant amount of A-type carbonate. We interpret these data as indicative of a greater ratio of A-type substitution for the barium and lead apatites than that present in CCaApF, but clearly this interpretation is not definitive because of the large uncertainties associated with most of the occupancies.

Infrared spectra

The infrared spectra of the CBaApF and CPbApF samples with varying carbonate concentrations are shown in Figures 5 and 6, where the IR-active carbonate band (ν_3, asymmetric stretch) is about 90 cm^{-1} lower in frequency than the analogous band in CCaApF (Fig. 7). The peaks for CCaApF containing about 13 wt% carbonate appear at 1421 and 1465 cm^{-1} with a slight shoulder at about 1500 cm^{-1}, consistent with the assignment of peaks at 1420 and 1462 cm^{-1} to B-type carbonate (Rosseeva et al. 2008; Fleet et al. 2004; see summaries in Tacker 2008).

Comparison of the carbonate regions of CBaApF and CPbApF with that of CCaApF reveals that the peaks for the barium and lead apatites appear at lower frequencies. The low-frequency peaks in the carbonate band for CPbApF appear at 1330 and 1382 cm^{-1}, with a significant high-frequency shoulder from about 1420 to 1460 cm^{-1}. The peaks for CBaApF occur at 1400, 1418, 1435, and 1458 cm^{-1}. We interpret the high-frequency peaks in the spectra of both barium (1435 and 1458 cm^{-1}) and lead apatites (from 1420 to 1460 cm^{-1}) as the asymmetric stretch for A-type carbonate. Indeed, the ~1400 cm^{-1} region for the most carbonated CBaApF (Fig. 5) shows two sets of peaks, presumably a doublet for A-type carbonate at higher frequency than the doublet for B-type carbonate. This difference between the asymmetric carbonate stretching frequencies of A- and B-type substitution in calcium apatites has been well documented (Schramm et al. 2000; Tonegawa et al. 2010; Fleet et al. 2004). For example, Shi, et al. (2005) report A-type carbonate asymmetric stretching modes for dental enamel at 1452–1456,

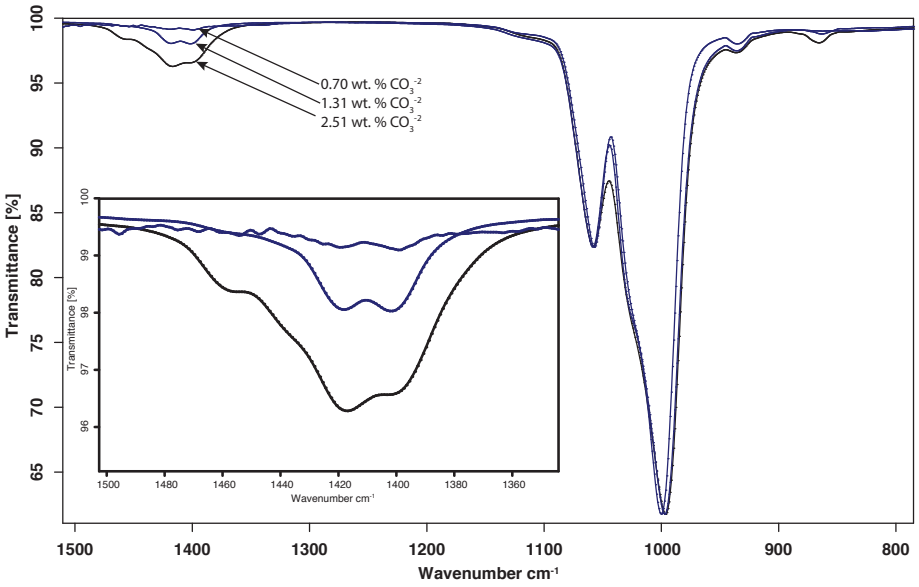

FIGURE 5. IR spectrum of CBaApF showing carbonate and phosphate bands in the region between 1500 and 900 cm^{-1}. The inset shows the carbonate region. (Color online.)

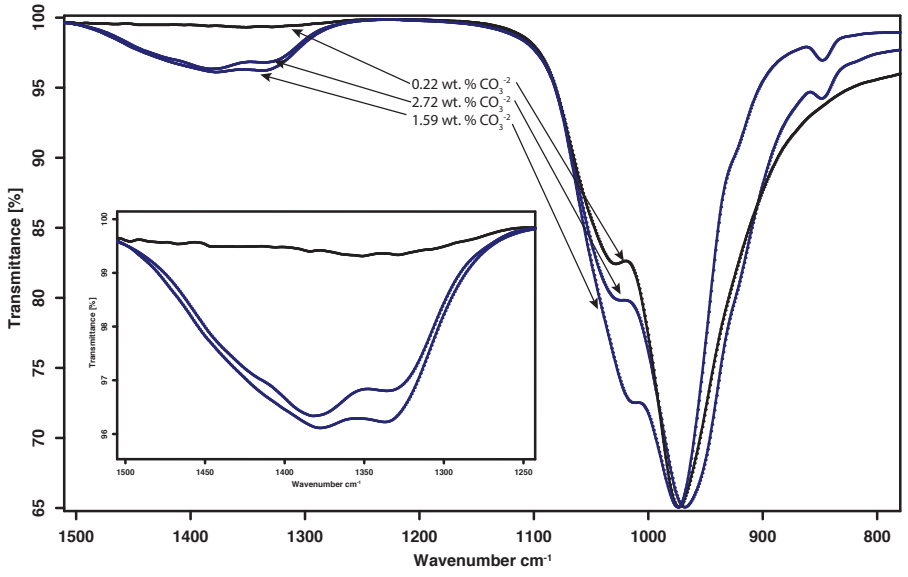

FIGURE 6. The infrared spectra of CPbApF samples from 700 to 1600 cm^{-1}. The inset shows the carbonate region. (Color online.)

1495–1501, and 1547–1451 cm^{-1} and B-type carbonate modes at 1412–1414 and 1469–1472 cm^{-1}. Tacker (2008) reports an average of literature B-type carbonate frequencies for synthetic calcium apatites as 1420 ± 6 and 1458 ± 5 cm^{-1}, and for A-type carbonate as 1462 ± 5 and 1535 ± 6 cm^{-1}. For geological apatites, Tacker (2008) reports averaged peak maxima of type B1 at 1409 ± 6 and 1450 ± 5 cm^{-1}, type B2 at 1427 ± 1 and 1460 ± 2 cm^{-1}, type A1 at 1539 ± 3 and 1475 ± 8 cm^{-1}, and type A2 at 1571 ± 3 and 1499 ± 5 cm^{-1}, and also stresses peak overlap as a source of error in reported peak frequencies.

In our spectra of the barium and lead fluorapatites, there is no suggestion of additional peaks that could be attributed to a second, conformationally distinct, A-type carbonate as suggested by Fleet and Liu (2003, 2004, 2005). The IR spectra of both the barium and lead fluorapatites show very weak broad peaks centered about 3400 cm^{-1}, attributable to water, but no peak at ca. 3570 cm^{-1} indicative of hydroxide ions.

Rationalization of cell parameters and substitution mode

Both Rietveld and IR analyses indicate a significant amount of A-type substitution in both CPbApF and CBaApF. For CPbApF, A-type substitution is also indicated by the increase in **a**- and

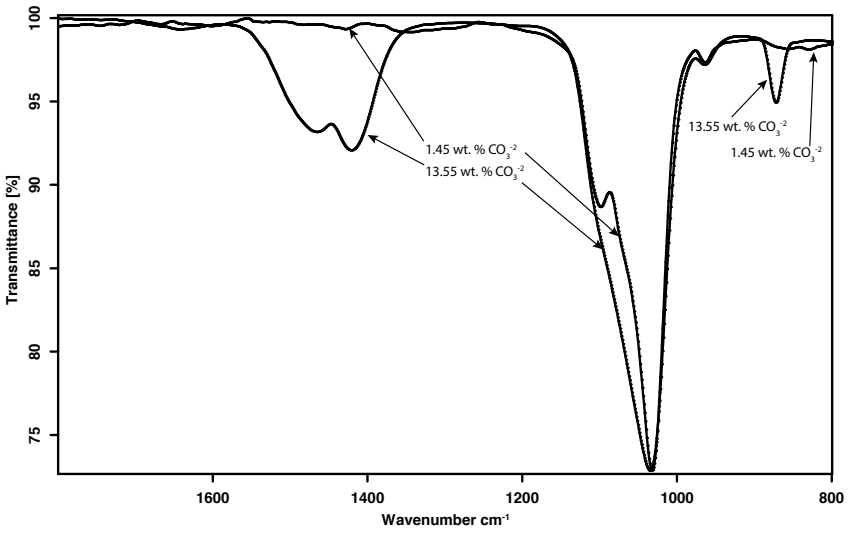

Figure 7. The IR spectra of CCaApF samples from 1800–750 cm^{-1}.

c-axis lengths as carbonate content increases. Although it is difficult to provide a more quantitative assessment, it is clear that the amount of A-type substitution in both of these carbonated barium and lead fluorapatites is greater than that present in CCaApF.

Association of the increase in **a**- and **c**-axis lengths for CPbApF with A-type carbonate substitution is consistent with the long-held belief that an increase in **a**-axis (but a slight decrease in **c**-axis) length in calcium apatites is due to the replacement of the monovalent anion (usually OH^- or F^-) with the larger carbonate ion (Holcomb and Young 1980; Elliot 2002; Fleet et al. 2004; Tonegawa et al. 2010). However, the clear dominance of B-type substitution in CPbApF seems to make this explanation less plausible. Assuming that the basic hexagonal structure of the apatite is maintained, the increase in both axial lengths must result from additional volume in the crystal structure necessitated by the increasing incorporation of the carbonate ion. Examination of atomic distances in the Rietveld-refined structures of CPbApF with 0.2 and 2.7 wt% carbonate shows that the primary differences lie in the distances between the triangularly disposed Pb(2) ions lying within planes perpendicular to the **c**-axis: the distance between these channel-defining ions is about 6% greater in the more carbonated apatite. By comparison, the closest distances between Pb(1) atoms are only 1.4% greater in the more-carbonated apatite. This analysis indicates widening of the channels, which correlates with the increase in the length of both axes. Such widening may result from replacement of fluoride by carbonate (A-type substitution). However, it also may be the case that greater B-type substitution produces a widening of the channels in the lead fluorapatites; that is, even when the carbonate ion does not occupy the channels, but substitutes for phosphate, the channels may widen significantly. Increased substitution of carbonate for phosphate with its concomitant development of fluoride vacancies within the channel may produce greater repulsions (due to loss of attraction to fluoride) between the channel-bounding lead ions. This channel expansion may be pronounced in CPbApF because of possible channel-delimiting, dative interactions between fluoride ions and the Lewis acidic lead cations, which would disappear as B-type substitution occurs. The same explanation may account for the observed (Sternlieb et al. 2010) increase in the **a**-axis length with increasing carbonate incorporation in CPbApOH.

In contrast to the effect of carbonate on the **a**-axis length in CPbApF, the **a**-axis length of CBaApF decreases uniformly with an increase in carbonate substitution. For this Ba apatite both Rietveld analysis and infrared spectroscopy indicate that A-type carbonate substitution is a substantial portion of the total substitution, but less than that in the lead analog. The decrease in the **a**-axis length in CBaApF (in which the proportion of A-type substitution is less than that in the lead analog) with increasing carbonate incorporation, can be explained by the smaller amount of A-type carbonate, by the absence of dative interactions of fluoride ions with the non-Lewis acidic barium ions, or by both effects.

Our IR and Rietveld analyses suggest that A-type carbonate substitution is more prevalent in barium and lead fluorapatites than in the smaller cation analog CCaApF, an observation that can be rationalized by the larger channels present in the barium and lead compounds. The differences in volume available in the channel can be estimated in two dimensions by considering one plane of M(2) ions. The areas of the arcs produced by the M(2) ions, obtained using standard formulas along with 6-coordinate ionic radii (Shannon 1976) and the 60° angle within the arc, are subtracted from the area of the triangle. The resulting "free space" in two dimensions provides an estimate of the space within the M(2) triangles in the absence of a monovalent anion. Using distances obtained from the structures of CaApF (Wyckoff 1965) and BaApF (Mathew et al. 1979) we estimate their free areas to be 4.6 and 5.5 $Å^2$, respectively, an increase in area of 20% in moving from Ca^{2+} to Ba^{2+}. Thus, we assume that A-type substitution is either more energetically favorable or kinetically more viable for apatites that contain larger cations.

Modeling studies of the relative stabilities of the A- and B-type carbonate sites in CCaApOH at 37 °C indicate that A-type (and mixed AB-type) carbonate substitution is energetically more

favorable than B-type (Peroos et al. 2006). Assuming that the presumably greater electrostatic interactions in the channel favor A-type substitution even in apatites with larger cations, we speculate that in the compounds prepared here, which contain larger cations, A-type substitution is thermodynamically favored. Why, then, do not all apatites, regardless of cation size, contain carbonate only in the channel (though one could imagine compounds with apatitic structures that could contain either extremely large cations or cations of lower charge where the channel site would not be energetically favored)? The answer may lie in the rate of the carbonate-incorporating reaction; that is, the rate at which carbonate substitutes for phosphate may be greater than the rate at which it substitutes for monovalent channel ions during the formation of the carbonated apatite. If these assumptions are correct, they also seem to suggest that during the formation of the carbonated apatite, the channel structure has already formed before the carbonate enters the mechanistic sequence.

It is also possible that B-type carbonate substitution is favored for most apatites formed in aqueous solution for thermodynamic reasons. Thermochemical analysis of substitution requires an assumption about the charge-balance mechanism involved in those substitutions. We find no evidence from Raman, IR, or XRD for the incorporation of sodium in our products. We have also done sodium analyses for calcium apatites prepared with the same procedure used for the syntheses of the barium apatites and have found only ca. 1% sodium in those products. Moreover, the changes in occupancies observed in our Rietveld analysis are consistent with dominant B-type substitution involving creation of calcium and fluoride vacancies. The equations for the most common substitution mechanisms for A-type and B-type carbonate are shown below for the substitution of one mole of carbonate per mole of apatite.

A-type: $M_{10}(PO_4)_6F_2(s) + CO_3^{2-}(aq) \rightarrow M_{10}(PO_4)_6(CO_3)(s) + 2\ F^-(aq)$

B-type: $M_{10}(PO_4)_6F_2(s) + CO_3^{2-}(aq) \rightarrow M_9(PO_4)_5(CO_3)F(s) + M^{2+}(aq) + PO_4^{3-}(aq) + F^-(aq)$

Subtraction of the second equation from the first produces:

$$\underset{\text{B-type}}{M_9(PO_4)_5(CO_3)F(s)} + M^{2+}(aq) + PO_4^{3-}(aq) \rightarrow \underset{\text{A-type}}{M_{10}(PO_4)_6(CO_3)(s)} + F^-(aq)$$

which represents the relative "stability" of B-type substitution of one carbonate for phosphate compared to A-type substitution of one carbonate for two fluorides in solution (assuming the charge compensation mechanism shown). The Gibbs energy change for this reaction could be estimated in several ways, one of which is to calculate the lattice enthalpy of both $M_9(PO_4)_5(CO_3)F(s)$ and $M_{10}(PO_4)_6(CO_3)(s)$ and then determine the enthalpy of hydration of the resultant gaseous ions [which form the solvated $M^{2+}(aq)$, $PO_4^{3-}(aq)$, and $F^-(aq)$ ions in the equation above]. The resultant $\Delta H°$ could then be converted to $\Delta G°$ using standard techniques for estimating absolute entropies. The lattice enthalpy for A-type apatite can with some certainty be assumed to be greater (meaning that the potential energy of the A-type apatite is lower and therefore it is more stable) than that of B-type apatite. This assertion rests on the greater number of more highly charged ions in the A-type lattice and the results of molecular dynamics calculations (Peroos et al. 2006). If the enthalpies of hydration of the M^{2+}, PO_4^{3-}, and F^- ions are ignored, the $\Delta H°$ (and $\Delta G°$) for the equation above could be assumed to be negative and the formation of A-type apatite in solution could be assumed to be favorable with respect to B-type apatite at least under conditions where the concentrations of the ions in solution are similar.

Our experimental work indicates that for barium and lead fluorapatites B-type substitution is favorable, but less so than for the calcium analog. This difference could be explained by the differences in enthalpies of hydration of the cations (the anions need not be considered because they will be the same no matter what cation is being considered), which in kJ/mol are Ca^{2+} = –1577, Ba^{2+} = –1305, Pb^{2+} = –1481 (Smith 1977). The Gibbs energies of hydration also vary inversely with the ionic radii of the ions (Latimer et al. 1939). The enthalpies (and Gibbs energies) of hydration therefore make $\Delta G°$ for the equation above less favorable for those apatites that contain cations with the most negative enthalpies of hydration. Thus, the greater amount of A-type carbonated apatite for barium and lead fluorapatite compared to calcium fluorapatite can be attributed to the less negative enthalpy (and Gibbs energy) of hydration of the larger Ba^{2+} and Pb^{2+} ions.

The greater percentage of carbonate that resides in the channel sites of the barium and lead fluorapatites, relative to that of carbonated calcium fluorapatite, can therefore be attributed to an increased rate of incorporation into the more spacious barium and lead cation channels and/or to the thermodynamically determinant effect of the solvation of the cations. We are continuing to study the consequences of these and similar observations.

Implications

Our work provides structural observations and principles that can be used to understand the incorporation of carbonate in compounds in the apatite family that vary in the size and chemical nature of the cations present. These principles, in turn, are of value in the interpretation of unit-cell parameters, particularly their variation with carbonate content, differences in occupancies of different substitution sites, and the nature/importance of the channel structure of apatites. We have shown that apatites with cations larger than calcium may incorporate carbonate more readily in the A- (channel) site and that an increase in the relative amount of A-type substitution is not necessarily revealed experimentally by an increase in the length of the **a**-axis. We have also provided a thermochemical analysis that can be used for any apatite to understand the relative energetics of A- vs. B-type carbonate substitution. These principles may be of value in understanding the composition and compositional variation within bone and tooth material and in the design of apatites that, by virtue of different substitution patterns, may have properties that are of value in, for example, the remediation of heavy metal contamination or the encapsulation of nuclear waste.

Acknowledgments

The authors acknowledge the Lucille and William Hackman Research Endowment at Franklin and Marshall College and the Center for Materials Innovation at Washington University for partial funding of this study. This material is based upon work supported by the National Science Foundation under Grant No. 0923224. We are also indebted to Linh Tran and Molly Carney for technical assistance and to the reviewers for their insightful comments.

REFERENCES CITED

Astala, R., and Stott, M.J. (2005) First principles investigation of mineral component of bone: CO_3 substitutions in hydroxyapatite. Chemistry of Materials, 17, 4125–4133.

Awonusi, A., Morris, M.D., and Tecklenburg, M.M.J. (2007) Carbonate assignment and calibration in the Raman spectrum of apatite. Calcified Tissue International, 81, 46–52.

Bhatnagar, V.M. (1970) Preparation, lattice parameters and X-ray powder patterns of lead fluorapatite and lead chlorapatite. Inorganic and Nuclear Chemistry Letters, 6, 913–917.

Belokoneva, E.L., Troneva, E.A., Dem'yanets, L.N., Duderov, N.G., and Belov, N.V. (1982) The crystal structure of synthetic fluoropyromorphite $Pb_5(PO_4)_3F$. Kristallografiya, 27, 793–794.

Beshah, K., Rey, C., Glimcher, M.J., Schimizu, M., and Griffin, R.G. (1990) Solid state carbon-13 and proton NMR studies of carbonate containing calcium phosphates and enamel. Journal of Solid State Chemistry, 84, 71–81.

Elliott, J.C. (1994) Structure and chemistry of the apatites and other calcium orthophosphates. Studies in Inorganic Chemistry, 18, p. 213–259. Elsevier, New York.

——— (2002) Calcium phosphate biominerals. In M.J. Kohn, J. Rakovan, and J.M. Hughes, Eds, Phoshates—Geochemical, geobiological, and materials importance, 48, p. 427–453. Reviews in Mineralogy and Geochemistry, Mineralogical Society of America, Chantilly, Virginia.

Fleet, M.E., and Liu, X. (2003) Carbonate apatite type A synthesized at high pressure: new space group (*P*3) and orientation of channel carbonate ion. Journal of Solid State Chemistry, 174, 412–417.

——— (2004) Location of type B carbonate ion in type A-B carbonate apatite synthesized at high pressure. Journal of Solid State Chemistry, 177, 3174–3182.

——— (2005) Local structure of channel ions in carbonate apatite. Biomaterials, 26, 7548–7554.

Fleet, M.E., Liu, X., and King, P.L. (2004) Accommodation of the carbonate ion in apatite: an FTIR and X-ray structure study of crystals synthesized a 2–4 GPa. American Mineralogist, 89, 1422–1432.

Flora, N.J., Hamilton, K.W., Schaeffer, R.W., and Yoder, C.H. (2004) A comparative study of the synthesis of calcium, strontium, barium, cadmium, and lead apatites in aqueous solution. Synthesis and Reactivity of Metal-Organic Compounds, 34, 503–521.

Holcomb, D.W., and Young, R.A. (1980) Thermal decomposition of human tooth enamel. Calcified Tissue International, 31, 189–201.

Ikoma, T., Kubo, Y., Yamazaki, A., Akao, M., and Tanaka, J. (2000) Effect of carbonate contents on crystal structure of A-type carbonate apatites. Key Engineering Materials. 192, 191–194.

Latimer, W.M., Pitzer, K.S., and Stansky, C.M. (1939) The free energy of hydration of gaseous ions, and the absolute potential of the normal calomel electrode, Journal of Chemical Physics, 7, 108–111.

Le Bail, A. (2004) Monte Carlo indexing with McMaille. Powder Diffraction, 19, 249–254.

LeGeros, R.Z., Trautz, O.R., Klein, E., and LeGeros, J.P. (1969) Two types of carbonate substitution in the apatite structure. Experimentia, 25, 5–7.

Liu, X., Shieh, S.R., Fleet, M.E., and Akhmetov, A. (2008) High-pressure study on lead fluorapatite. American Mineralogist, 93, 1581–1584.

Mathew, M., Mayer, I., Dickens, B., and Schroeder, L.W. (1979) Substitution in barium-fluoride apatite: the crystal structures of $Ba_{10}(PO_4)_6F_2$, $Ba_6La_2Na_2(PO_4)_6F_2$ and $Ba_4Nd_3Na_3(PO_4)_6F_2$. Journal of Solid State Chemistry, 28, 79–95.

Meegoda, C., Bonner, C.E., Loutts, G., Stefanos, S., and Miller, G.E. III (1999) Raman spectroscopic study of barium fluorapatite. Journal of Luminescence, 81, 101–109.

Nassif, N., Martineau, F., Syzgantseva, O., Gobeaux, F., Willinger, M., Coradin, T., Cassaignon, S., Azaïs, T., and Giraud-Guille, M.M. (2010) Chemistry of Materials, 22, 3653–3663.

Nelson, D.G.A., and Williamson, B.E. (1982) Low-temperature laser Raman spectroscopy of synthetic carbonated apatites and dental enamel. Australian Journal of Chemistry, 35, 715–727.

Nriagu, J.O. (1984) Formation and stability of base metal phosphates in soils and sediments. In J.O. Nriagu and P.B. Moore, Eds., Phosphate Minerals, p. 318–329. Springer-Verlag, New York.

Pan, Y., and Fleet, M.E. (2002) Composition of the apatite-group minerals: substitution mechanisms and controlling factors. In M.J. Kohn, J. Rakovan, and J.M. Hughes, Eds., Phosphates—Geochemical, geobiological, and materials importance, 48, p. 13–49. Reviews in Mineralogy and Geochemistry, Mineralogical Society of America, Chantilly, Virginia.

Pasteris, J.D., Yoder, C.H., Sternlieb, M.P., and Liu, S. (2012) Effect of carbonate incorporation on the hydroxyl content of hydroxylapatite. Mineralogical Magazine, 76, 2741–2759.

Pasteris, J.D., Yoder, C.H., and Wopenka, B. (2014) Molecular water in nominally unhydrated carbonated hydroxylapatite: the key to a better understanding of bone mineral. American Mineralogist, 99, 16–27.

Penel, G., Leroy, G., Rey, C., and Bres, E. (1998) MicroRaman spectral study of the PO_4 and CO_3 vibrational modes in synthetic and biological apatites. Calcified Tissue International, 63, 475–481.

Peroos, S., Du, Z., and de Leeuw, N.H. (2006) A computer modeling study of the uptake, structure and distribution of carbonate defects in hydroxyl-apatite. Biomaterials, 27, 2150–2161.

Resende, N.S., Nele, M., and Salim, V.M.M. (2006) Effects of anion substitution on the acid properties of hydroxyapatite. Thermochimica Acta, 451, 16–21.

Rey, C., Renugopalakrishnan, V., Collins, B., and Glimcher, M.J. (1991) Fourier transferom infrared spectroscopic study of the carbonate ions in bone mineral during aging. Calcified Tissue International, 49, 251–258.

Rosseeva, E.V., Buder, J., Simon, P., Schwarz, U., Frank-Kamenetskaya, O.V., and Kniep, R. (2008) Synthesis, characterization, and morphogenesis of carbonated fluorapatite-gelatine nanocomposites: a complex biomimetic approach toward the mineralization of hard tissues. Chemistry of Materials, 20, 6003–6013.

Ruby, M.V., Davis, A., and Nicholson, A.D. (1994) In situ formation of lead phosphates in soils as a method to immobilize lead. Environmental Science and Technology, 28, 646–654.

Shannon, R.D. (1976) Revised effective ionic-radii and systematic studies of interatomic distances in halides and chalcogenides. Acta Crystallographica Section A, 32, 751–767.

Schramm, D.U., Terra, J., Rossi, A.M., and Ellis, D.E. (2001) Configuration of CO_2(-) radicals in gamma-irradiated A-type carbonated apatites: theory and experimental EPR and ENDOR studies. Physical Review B, 63, 1–14.

Shi, J., Klocke, A., Zhang, M., and Bismayer, U. (2005) Thermally-induced structural modification of dental enamel apatite: decomposition and formation of carbonate groups. European Journal of Mineralogy, 17, 769–775.

Smith, D.W. (1977) Ionic hydration enthalpies, Journal of Chemical Education, 54, 540–541.

Sternlieb, M.P., Pasteris, J.D., Williams, B.R., Krol, K.A., and Yoder, C.H. (2010) The structure and solubility of carbonated hydroxyl- and chloro lead apatites. Polyhedron, 29, 2364–2372.

Sudarsanan, K., Mackie, P.E., and Young, R.A. (1972) Comparison of synthetic and mineral fluorapatite, $Ca_5(PO_4)_3F$, in crystallographic detail. Materials Research Bulletin, 7, 1331–1338.

Tacker, R.C. (2008) Carbonate in igneous and metamorphic fluorapatite: two type A and two type B substitutions. American Mineralogist, 93, 168–176.

Tonegawa, T., Ikoma, T., Yoshioka, T., Hanagata, N., and Tanaka, J. (2010) Crystal structure refinement of A-type carbonate apatite by X-ray powder diffraction. Journal of Material Science, 45, 2419–2426.

Traina, S.J., and Laperche, V. (1999) Contaminant bioavailability in soils, sediments, and aquatic environments. Proceedings of the National Academy of Sciences, 96, 3365–3371.

Werner, P.-E., Eriksson, L., and Westdahl, M.J. (1985) Treor, a semi-exhaustive trial-and-error powder indexing program for all symmetries. Journal of Applied Crystallography, 18, 367–370.

Wilson, R.M., Elliott, J.C., Dowker, S.E.P., and Smith, R.I. (2004) Rietveld structure refinement of precipitated carbonate apatite using neutron diffraction data. Biomaterials, 25, 2205–2213.

Wilson, R.M., Elliott, J.C., Dowker, S.E.P., and Rodriguez-Lorenzo, L.M. (2005) Rietveld refinements and spectroscopic studies of the structure of Ca-deficient apatite. Biomaterials, 26, 1317–1327.

Wilson, R.M., Dowker, S.E.P., and Elliott, J.C. (2006) Rietveld refinements and spectroscopic structural studies of a Na-free carbonate apatite made by hydrolysis of monetite. Biomaterials, 27, 4682–4692.

Wopenka, B., and Pasteris, J.D. (2005) A mineralogical perspective on the apatite in bone. Materials Science and Engineering C, 25, 131–143.

Wyckoff, R.W.G. (1965) Crystal Structures, 2nd ed., vol. 3, p. 228, Interscience, New York.

Yoder, C.H., Pasteris, J.D., Krol, K.A., Weidner, V.L., and Schaeffer, R.W. (2012) Synthesis, structure, and solubility of carbonated barium chlor- and hydroxylapatites. Polyhedron, 44, 143–149.

MANUSCRIPT RECEIVED DECEMBER 3, 2013
MANUSCRIPT ACCEPTED MAY 6, 2014
MANUSCRIPT HANDLED BY MICKEY GUNTER